Revista Iberoamericana de Ingeniería Mecánica. Vol. 28, N.º 2, pp. 15-25, 2024

X-rays and Corrosion Resistance Analysis of Super Duplex Stainless Steel UNS 32750

Análisis de resistencia a la corrosión y rayos X del acero inoxidable superdúplex UNS 32750

Dimitry V. Bubnoff[1], Mariana M.O. Carvalho[2]
[1]Fluminense Federal University
Departament of Metalurgical Engineering and Materials Science, Brazil
[2]Lappeenranta University of Technology, LUT, Finland

(Recibido 23 de enero de 2024, para publicación 15 de mayo de 2024)

Abstract – During heat treatment of distinct types of stainless steel, precipitation of undesirable phases may occur. resulting in reduction of corrosion resistance due to formation of regions depleted of Cr and Mo, as well as significant changes in mechanical properties. Corrosion resistance reduction and embrittlement caused by small volumetric fractions of sigma phase in the microstructure are widely discussed in the literature; however, a great variability in the results is observed. Thus, it becomes essential to study the sigma phase formation, aiming at predicting the microstructural changes after certain thermal history and consequently the corrosion resistance. In this work, the sigma phase formation was analyzed in two independent ways: X-rays of dilatometric trials and corrosion tests. The results show that phase transformations occur predominantly in the temperature range between 800°C and 900°C, where the sigma phase precipitation was observed in the steel UNS 32750.

Keywords – Super Duplex Stainless Steel, X-Ray Analysis, Corrosion Resistance.

Resumen – Durante el tratamiento térmico de distintos tipos de acero inoxidable, puede ocurrir la precipitación de fases indeseables, lo que resulta en una reducción de la resistencia a la corrosión debido a la formación de regiones empobrecidas en Cr y Mo, así como cambios significativos en las propiedades mecánicas. La reducción de la resistencia a la corrosión y la fragilización causada por pequeñas fracciones volumétricas de la fase sigma en la microestructura son ampliamente discutidas en la literatura; sin embargo, se observa una gran variabilidad en los resultados. Por lo tanto, se vuelve esencial estudiar la formación de la fase sigma, con el objetivo de predecir los cambios microestructurales después de cierta historia térmica y, en consecuencia, la resistencia a la corrosión. En este trabajo, la formación de la fase sigma se analizó de dos formas independientes: rayos X de ensayos dilatométricos y pruebas de corrosión. Los resultados muestran que las transformaciones de fase ocurren predominantemente en el rango de temperatura entre 800 ° C y 900 ° C, donde se observó la precipitación de la fase sigma en el acero UNS 32750.

Palabras clave – Acero inoxidable superdúplex, análisis de rayos X, resistencia a la corrosión.

1. INTRODUCTION

Processing of stainless steel alloys (*e.g.* heat treatment, welding, hot forming) or even during use (e.g. isothermal aging), intermetallic phase precipitation may occur, such as phases chi (χ), alpha prime (α'), sigma (σ), besides carbonates and nitrates. This phenomenon is often attributed to microstructural instabilities of steel alloys [1-3]. Particularly between 700ºC and 900ºC, phase sigma formation may occur via three distinct mechanisms: as a product formed from the eutectoid decomposition of the original ferrite, which also generates secondary austenite; through nucleation and further growth process from the original ferrite; or from the austenite present, after all ferrite has been consumed [4-5].

The phase (σ) precipitation is especially relevant for austenitic, ferritic, and Duplex stainless-steel alloys, because it is usually associated with hindering of mechanical properties, as well as the decreasing corrosion

resistance [6-7]. On the other hand, thermal treatment parameters, are important for AID/AISD alloys, because their properties are strongly influenced by microstructural transformations resulting from thermal cycles [8-10]. Thus, the evaluation of such heat treatment parameters and the understanding of condition under which the phase sigma is formed are substantial to enhance the stainless-steel properties and progress on its utilization [11-13].

2. MATERIALS AND METHODS

The X-ray diffractograms (XRD) of the samples treated at 700°C, 750ºC, 800ºC and 900ºC were collected using a Bruker-D4 Endeavor from the CETEM Laboratory (Mineral Technology Center/RJ). Cross section analyses of the proof bodies were conducted in the following operating conditions: Co Kα radiation, goniometer speed of 0.02º per 2θ per step with counting time of 1 second per step, collected from 40º to 80º 2θ. The X-ray source was exited at 35 kV and 40 mA. The qualitative interpretation of the collected spectra was based on comparison with standards taken from the database PDF02 (ICDD, 2006) from the software Bruker AXS Diffraction Plus.

The XRD analysis was performed not only to show the presence of distinct phases in the samples, but also to evaluate the use of this method to quantify the phases and possibly observe peak displacement caused by deformation.

The potentiodynamic anodic polarization analysis was done with a Potentiostat-Galvanostat Solartron, using a Ag/AgCl reference electrode and a Platinum auxiliary electrode. The tests were performed in 3.0% aqueous NaCl solution at ambient temperature, varying potential from -0.2 to +1.2 V with scanning speed of 5 mV/s, as per ASTM G48-03 standard.

Electrochemical measurements were made in a single compartment conventional electrochemical cell, built in the Electrochemistry and Corrosion Laboratory at FEG/UNESP. The anodic and cathodic branches were obtained simultaneously. The potential scanning range started at -0.3 V below the open circuit potential (E_{OC}) up to a potential above the passive layer rupture. From these tests, it is possible to assess the corrosion speed, self-passivation tendency, and the potential range in which the material remains passive.

Tabel 1. Analyzed chemical composition of super duplex steel UNS 32750/SAF 2507 (% by weight). Sandvik.

C	Mn	Si	P	S	Cr	Ni	Mo	Cu	N
0,0205	0,85	0,328	0,0267	0,0009	24,89	6,82	3,72	0,156	0,278

3. RESULTS AND DISCUSSION

3.1. X-ray tests

The diffraction peaks corresponding to the planes of each phase were compared against each other during the measurements. The corresponding planes of each peak were indicated: γ (111), δ (110), γ (200), δ (200).

Fig. 1 shows the diffraction result of the original metal sample, i.e. before heat treatment. It is possible to observe that the only phases present in the sample are austenite and ferrite. This result was already expected, because without suffering any thermal treatment the material does not exhibit precipitation of secondary phases or they are present in quantities below the X-ray detection limit.

All the intensity curves given as a function of the diffraction angle showed similar behavior and the peaks presented are mainly related to the ferrite and austenite phases. However, in the samples submitted to treatment at 700ºC, 750ºC, 800ºC and 900ºC, the intermetallic sigma phase was also found, as identified in the graphs below.

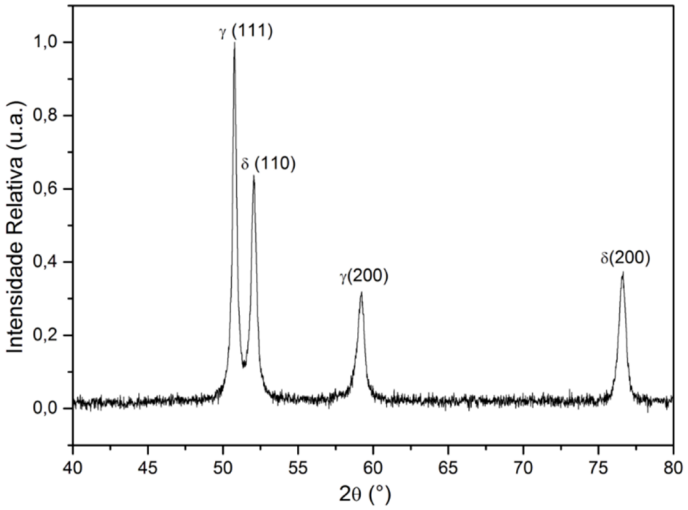

Fig. 1. X-ray diffractogram of the original sample.

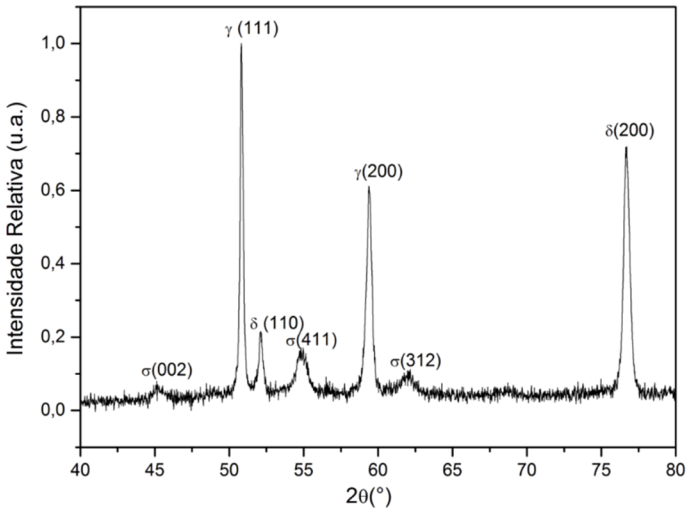

Fig. 2. X-ray diffractogram of the sample submitted to 700ºC.

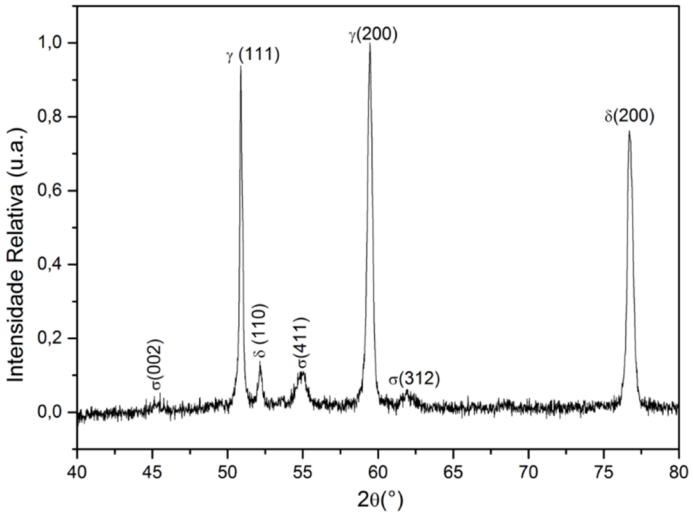

Fig. 3. X-ray diffractogram of the sample submitted to 750ºC.

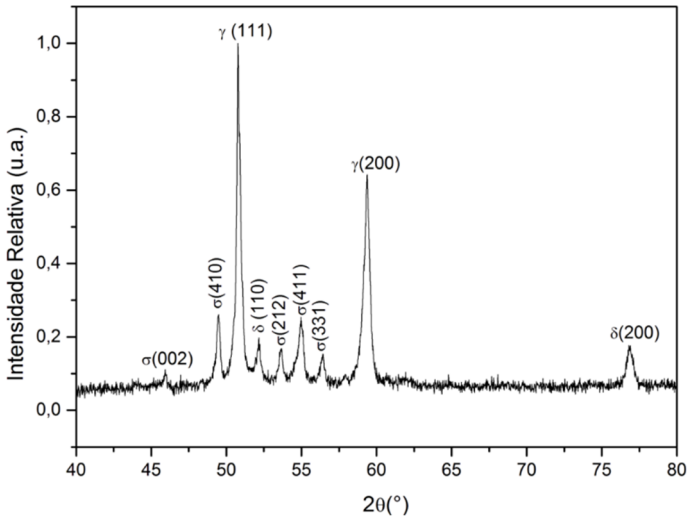

Fig. 4. X-ray diffractogram of the sample submitted to 800ºC.

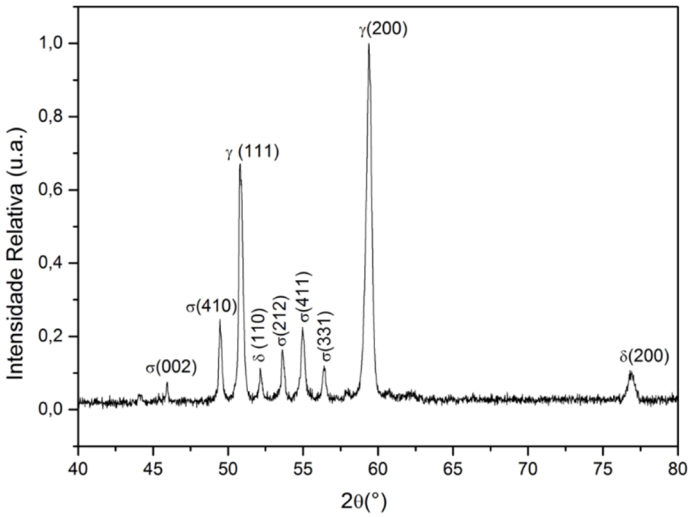

Fig. 5. X-ray diffractogram of the sample submitted to 900ºC.

For the lowest temperatures (*i.e*. 700°C and 750°C samples), the sigma phase appears in minor quantities, whereas for higher temperatures the development of the sigma phase is clear. It should be noted that, for a soak time of 60 minutes, the sigma phase development occurs at 800°C. From 800°C to 900°C no significant changes were observed in the amount of the secondary phase. By following the appearance of the sigma phase, a decrease in the amount of ferrite was observed.

Figures 2 to 5 show the diffracted peaks as a function of the angular interval in 2θ for different heat treatment conditions. Between 50° and 52°, it can be observed that the peak corresponding to ferrite δ (110), initially with high intensity, decreases as temperature increases. These results also show that the peaks corresponding to the deleterious phases increase as the temperature increases, which agrees with the results presented by Pardal *et al*. [14].

According to the results of the analysis, a mixed crystalline structure composed of two phases, austenite and ferrite, are present in this steel, in close proportions, as verified by the amounts and intensities of the peaks presented in the diffraction pattern This characteristic of the duplex steels, also observed in the work of Tan *et al*. [15], confers the material an attractive combination of mechanical properties and resistance to corrosion.

3.2. Open-circuit Potential (OCP)

The immersion potential can be influenced by several reasons, from simpler ones such as sanding time of the sample and sandpaper size, to most important causes such as the time between sanding and testing, and especially the concentration of Cr (or oxide) and the distribution of this element in the surface. For these reasons, when analyzing the OCP curves, observing the curve trends is more important than absolute numerical values.

Fig. 6 shows the OCP curves of the Super Duplex steel in NaCl solution 3.0 % and pH 6.0, obtained for 15 hours, subjected to different thermal treatments, scanning speed 5 mV/sec.

A tendency of samples of 750°C and 800°C to form a passive layer can be observed, which is revealed by an increasing (more positive) potential. After about 5 hours a potential decrease is observed, indicating the breakdown of the passive layer. The potential tends to stabilize at about -0.12 V. The curve obtained from the sample treated at 900°C shows a potential increase in the first 50 minutes and then a decrease of this parameter until it reaches -0.16 V. The sample at 700°C reveals only a potential decrease, stabilizing at about -0.19 V.

Although distinct behaviors were observed in the curves for different thermal treatment temperatures, the open circuit potential values, after 15 h do not vary more than 0.07 V. This small potential difference observed in the samples may be associated with the presence of Cr-rich phases resulting from the thermal treatment applied, which may form micropiles due to the potential difference in relation to the matrix. The curve obtained for sample treated at 800ºC, which has a greater percentage of the sigma phase in its microstructure, exhibits multiple oscillations, indicating the sample is being actively corroded and with difficulty to passivate itself.

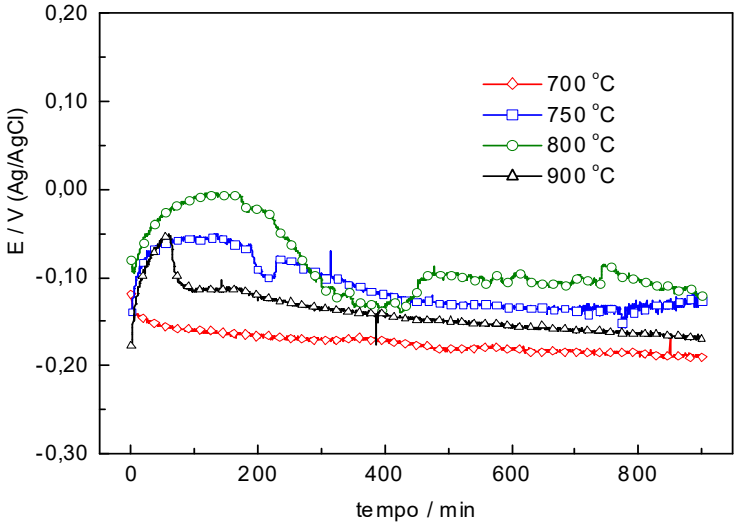

Fig. 6. OCP for different thermal treatments, in 3.0 % NaCl solution and pH 6.0.

3.3. Cyclic Voltammetry Test (CV)

Fig. 7 shows the cyclic voltammetry curves, dilatometry overlap, scanning speed 5mV/s. In the anodic scan, towards the positive potential, two oxidation peaks are observed for the sample treated at 750ºC. The first peak with the negative potential (-0.1 V) can be associated with Fe (II) oxidation, the second with the positive potential, +0.2 V, can be related to the oxidation of Fe (II) to Fe (III). In the range of +0.2 V to +1.2 V there is a passive region, linked to the protective layer stability. After 1.2 V the current began to increase, which indicates that the increase of potential would break the protective layer, causing the dissolution of the material. For this reason, the inverse (cathodic) sweep was initiated, represented by the turning curve. It can be concluded that the value +1.2 V is the potential limit for sample 750ºC.

Unlike the positive scan, the negative scan curve displays no peaks because the sweep passes through the area where the surface has already been passivated. However, the peak at -0.18 V indicates a reduction process, which can be explained by the fact that, during the positive sweep, this area between -0.1 V and

+0.2 V was transformed. In other words, as the oxidation process is irreversible – it is not possible to reduce everything that was oxidized during the anodic sweep – the oxidation area represented by the two peaks between -0.1 V and +0.2 V, is larger than the peak area in the cathodic scan.

The curves corresponding to the samples treated at 700ºC, 800ºC and 900ºC present a passive region in the anodic scan. After the rupture of the passive layer and reversal of the scanning direction, a re-oxidation current is observed, with peaks in the range of +0.1 V to +0.2 V. The peaks are related to the oxidation of the metal, in the same way as discussed for the sample treated at 750°C. However, this process becomes more evident for the samples treated at 800°C and 900°C. For these samples, the current magnitude higher, which indicates that the re-passivation, after rupture of the protective layer and the inversion of the scanning direction, does not occur. The increase in current in the cathodic scan is a result of the higher reactivity of the metal and an increase of the active area when the passive layer is ruptured.

The lower current values translate into better resistance against corrosion. As observed i.7, the dilatometric samples treated at 800ºC and 900ºC with current values of 0.001 A and 0.0004 A, respectively, are more propense to corrosion compared to the samples treated at 700°C and 750°C, in which the current is very low.

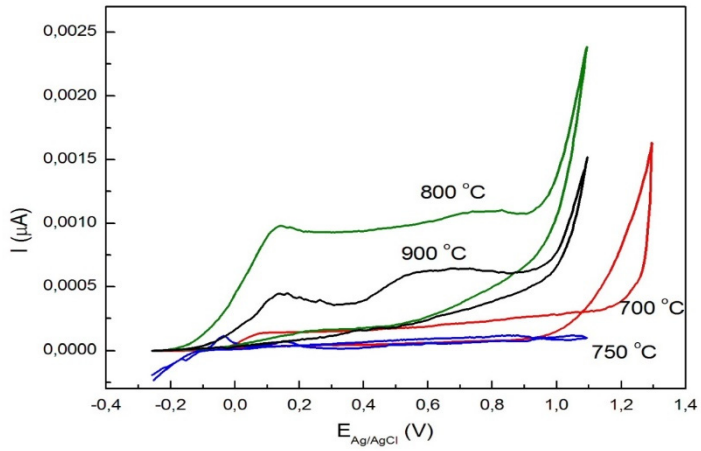

Fig. 7. Cyclic voltammetry curves, dilatometry overlap, scanning speed 5mV/s.

3.4. Tafel test

In the analysis of the potentiodynamic polarization curves (Tafel curves), the values of current density (j_{corr}) in the corrosion potential (E_{corr}), passivation current density (j_{pass}) and passive layer rupture potential (E_{rup}) are obtained. These parameters allow the evaluation of resistance to corrosion, while providing information about the behavior (active, passive or pseudo-passive) and the mechanism that controls the corrosion process of different materials in a specific medium.

Fig. 8 shows the Tafel curves for the samples of Super Duplex steel subjected to different thermal treatments (dilatometry tests) at 700°C, 750°C, 800°C and 900°C in 3.0% NaCl solution, pH 6.0, obtained at a potential scanning speed of 0.33 mV / s (20 mV / min).

An increase in the current I (A) expresses a decrease in corrosion resistance, evidencing that, among the specimens submitted to the dilatometry tests, the most protected samples are those treated at 700ºC and 750ºC, as they presented the lowest current density values. This response is consistent with the results of X-rays.

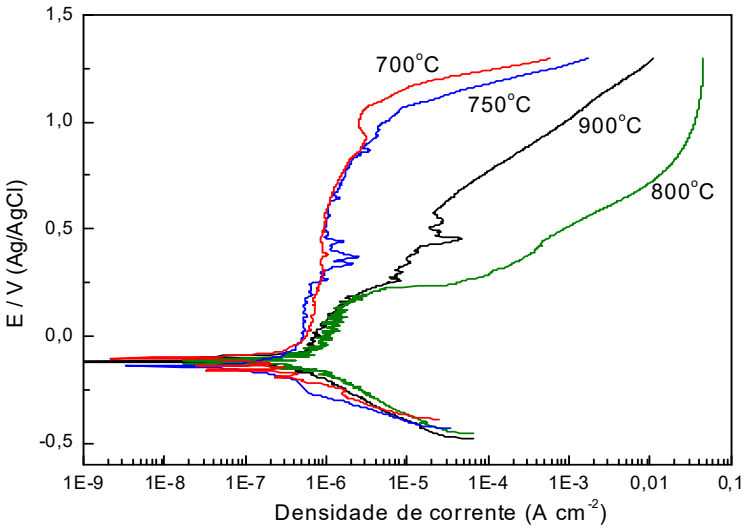

Figure 8 – Tafel curves overlapping dilatometry, scanning speed 5 mV/s.

It is also possible to notice that the samples treated at 700°C and 750°C have a wide passive region from -0.1V to +1.1V, above which the passive layer ruptures. On the other hand, the samples treated at 800°C and 900°C have a much lower passive region raging from -0.1V to +0.2V. Above this potential, the rupture of the passive layer occurs, and the dissolution of the metal begins. The extent of the passivity region is defined by the volume of sigma phase in the microstructure, which decreases the protection region and consequently the corrosion resistance.

In Table 2 the corrosion parameters obtained from the Tafel curves are presented: corrosion potential (E_{corr}), corrosion current density (j_{corr}), passivation current density (j_{pass}) obtained at 0.15 V and potential of rupture (E_{rup}).

Table 2. Corrosion parameters E_{corr}, j_{corr}, j_{pass} and E_{rup} obtained for super duplex SAF 2507 after different thermal treatments.

	E_{corr} (V)	j_{corr} (A cm^{-2})	j_{pass} (A cm^{-2}) (E = 0,15 V)	E_{rup} (V)
700 °C	-0,110	1,2 x 10^{-7}	7,1 x 10^{-7}	+1,09
750 °C	-0,141	1,2 x 10^{-7}	5,3 x 10^{-7}	+1,05
800 °C	-0,123	5,6 x 10^{-7}	1,8 x 10^{-6}	+0,16
900 °C	-0,122	3,0 x 10^{-7}	1,5 x 10^{-6}	+0,21

The oscillations observed in all the figures are a sign of rupture of the passive layer and immediate re-passivation, or reconstruction of this layer, which is unambiguous evidence of localized corrosion.

4. CONCLUSIONS

The XRD analysis did not detect any other phase in the UNS S32750/SAF 2507 steel, which influences the corrosion resistance, besides the sigma phase.

The resistance to corrosion is a direct function of the volume of sigma in its structure, the larger the volumetric fraction of sigma, the lower the resistance to corrosion of the material.

The presence of the sigma phase does not alter the corrosion potential of the steel UNS S32750/SAF 2507 in 3,0 % NaCl solution under the test conditions used in this study.

The thermal treatment parameters affected the behavior of the material in terms of corrosion resistance demonstrating difficulty of the samples above 800ºC in the passivity, probably due to the sigma phase morphology.

REFERENCES

[1] Örnek C. *et al.*, "Understanding passive film degradation and its effect on hydrogen embrittlement of super duplex stainless steel – Synchrotron X-ray and electrochemical measurements combined with CalPhaD and ab-initio computational studies", *Applied Surface Science*, 628, 157364 (2023)

[2] Wang, R., "Precipitation of sigma phase in duplex stainless steel and recent development on its detection by electrochemicalpotentiokinetic reactivation: a review", *Corrosion Communications*, 2, 41–54 (2021) DOI:10.1016/j.corcom.2021.08.001

[3] Wang, Q. *et al.*, "Investigation of microstructure evolution, mechanical and corrosion Properties of SAF2507 super duplex stainless steel joints by keyhole plasma arc welding", *Journal of Materials Research* and Technology, 22, 355–374 (2023)

[4] Cui, S. *et al.*, "Influence of Welding Speeds on the Morphology, Mechanical Properties, and Microstructure of 2205 DSS Welded Joint by K-TIG Welding", *Materials*, 14, 3426 (2021)

[5] Bubnoff D.V., "Estudo das transformações de fase em aço superduplex UNS 32750/SAF 2507. Tópicos abordados: soldagem, corrosão, caminho microestrutural e simulação", Tesis Doctoral, Universidade Federal Fluminense UFF, Rio de Janeiro (2015)

[6] Oñate, A. e*t al.*, Exploring the Impact of Cooling Rate on Microstructural Features, Mechanical Properties, and Corrosion Resistance of a Novel Nb-Stabilized Super Duplex Stainless Steel in Shielded Metal Arc Welding, *MDPI Crystals*, 13, 1192 (2023) https://doi.org/10.3390/cryst13081192

[7] Miranda-Pérez, A.F. *et al*., Corrosion Resistance of GMAW Duplex Stainless Steels Welds, *Materials*, 16, 1847 (2023)

[8] Hou, Y. *et al.*, "Initiation mechanism of pitting corrosion in weld heat affected zone of duplex stainless steel", *Corrosion Science*, 201, 110278 (2022)

[9] Murkute, P. *et al.*, "Effect of thermal aging on corrosion behavior of duplex stainless steels", SN *Applied Sciences*, 4, 97 (2022)

[10] *Practical Guidelines for the fabrication of duplex steel*. Third edition, ISBN 978-1-907470-09-7, London UK, (2015)

[11] Wang, Y., Sun, H., Li, N., Xiong, Y., Jing, H., "Effect of Sigma Phase Precipitation on the Pitting Corrosion Mechanism of Duplex Stainless Steels", *International Journal of Electrochemical Science*, 13, 9868-9887, (2018)

[12] HaiTao, Y., SenSen, X., Yong, Y., Sai, Y., MouCheng, Li., "Electrochemical Corrosion Behavior of 2205 Duplex Stainless Steel Welds in Chloride Solutions", *International Journal of Electrochemical Science*, 14, 1423-1433 (2019)

[13] Jiakun, S., Xiaolei, L., Yangting, S., Yiming, J., Jin, L., "A Study on the Pitting Initiation of Duplex Stainless Steel (DSS 2205) Welded Joints Using SEM–EDS, SKPFM and Electrochemistry Methods", *International* Journal *of Electrochemical Science*, 13, 11607–11619 (2018)

[14] Pardal, J.M. *et al.*, "Uma Revisão da Resistência à Corrosão em Aços Inoxidáveis Duplex e Super Duplex", *Rev. Virtual Quim*., **5**(4), 658-677 (2013)

[15] Tan, H. *et al.*, "Influence of welding thermal cycles on microstructure and pitting corrosion resistance of 2304 duplex stainless steel". *Corrosion Science*, 55, 368-377 (2012)

Attachments demonstrating some the tests carried out:

a) b)

Fig. 9. a) Potentiostatic assay system, b) sample preparation.

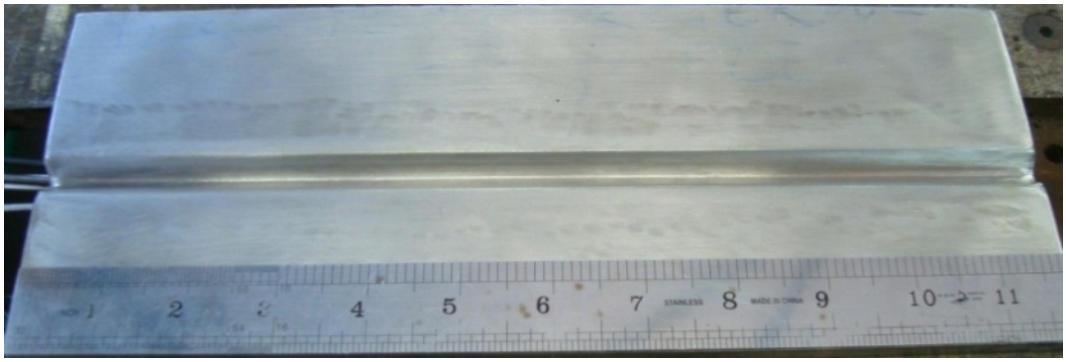

Fig. 10. Image of the machined sheet, before testing.

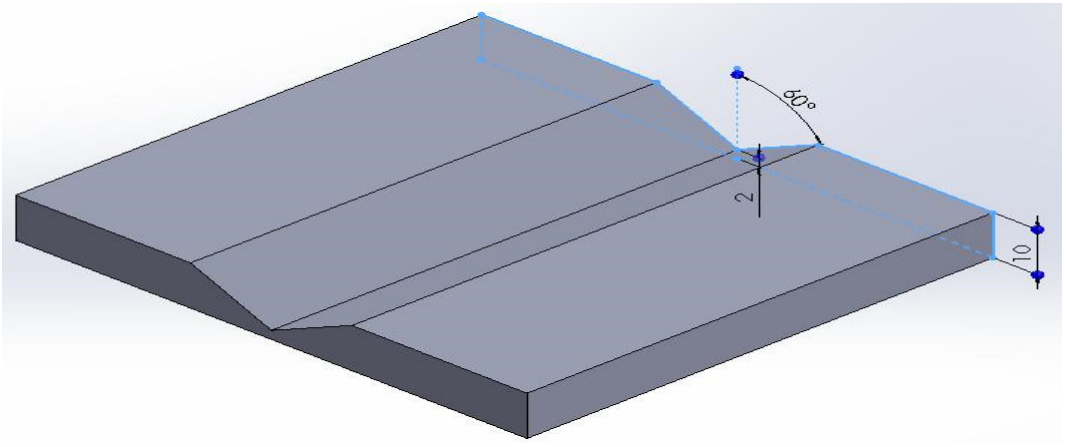

Fig. 11. Schematic presentation of V-chamfer.

Fig. 12. Positioning of termocouples for data collection.

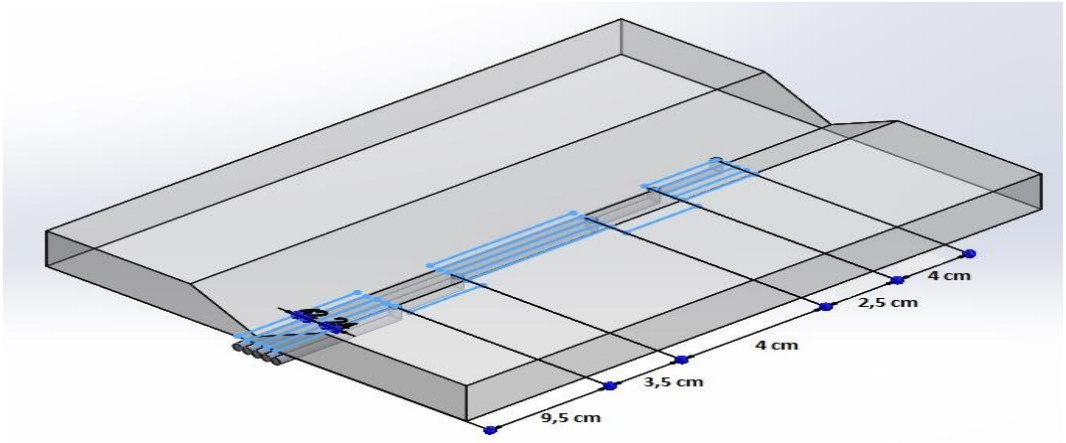

Fig. 13. Schematic presentation of termocouple positioning.

Fig. 14. Plate cutting section details.

Table 3. Mechanical properties, at 20ºC, in the annealed state and for a maximum thickness of 20 mm, UNS S32750/SAF 2507. (Sandvik)

Rp0,2(MPa) min.	Rm (MPa)	A (%) min.	HRC max.
550	800 – 1000	25	32

Table 4. Physical properties of UNS S32750/SAF 2507. (Sandvik)

Tipo	UNS	Specific heat J/kgK	Thermal conductivity W/mK	Linear thermal expansion coefficient 10^{-6} K^{-1}
Super duplex	S32750	470	20	14,0

Table 5. Corrosion rate of various alloys in 80% acetic acid with 2000 ppm chloride ions at 90ºC.

Corrosion rate mm/year	Steel
0,15	316L
0,025	SAF 2205
0,013	Sanicro 28
0,01	UNS S32750/SAF 2507